bioengineering

MDPI

Article

Gait Event Prediction Using Surface Electromyography in Parkinsonian Patients

Stefan Haufe [1,2,3,4,*], Ioannis U. Isaias [5,6], Franziska Pellegrini [3,4] and Chiara Palmisano [5]

[1] Uncertainty, Inverse Modeling and Machine Learning Group, Technical University of Berlin, 10587 Berlin, Germany
[2] Mathematical Modelling and Data Analysis Department, Physikalisch-Technische Bundesanstalt Braunschweig und Berlin, 10587 Berlin, Germany
[3] Berlin Center for Advanced Neuroimaging, Charité–Universitätsmedizin Berlin, 10117 Berlin, Germany
[4] Bernstein Center for Computational Neuroscience Berlin, 10115 Berlin, Germany
[5] Department of Neurology, University Hospital Würzburg and Julius-Maximilians-Universität Würzburg, 97080 Würzburg, Germany
[6] Centro Parkinson, ASST G. Pini-CTO, 20126 Milano, Italy
* Correspondence: haufe@tu-berlin.de

Abstract: Gait disturbances are common manifestations of Parkinson's disease (PD), with unmet therapeutic needs. Inertial measurement units (IMUs) are capable of monitoring gait, but they lack neurophysiological information that may be crucial for studying gait disturbances in these patients. Here, we present a machine learning approach to approximate IMU angular velocity profiles and subsequently gait events using electromyographic (EMG) channels during overground walking in patients with PD. We recorded six parkinsonian patients while they walked for at least three minutes. Patient-agnostic regression models were trained on temporally embedded EMG time series of different combinations of up to five leg muscles bilaterally (i.e., tibialis anterior, soleus, gastrocnemius medialis, gastrocnemius lateralis, and vastus lateralis). Gait events could be detected with high temporal precision (median displacement of <50 ms), low numbers of missed events (<2%), and next to no false-positive event detections (<0.1%). Swing and stance phases could thus be determined with high fidelity (median F1-score of ~0.9). Interestingly, the best performance was obtained using as few as two EMG probes placed on the left and right vastus lateralis. Our results demonstrate the practical utility of the proposed EMG-based system for gait event prediction, which allows the simultaneous acquisition of an electromyographic signal to be performed. This gait analysis approach has the potential to make additional measurement devices such as IMUs and force plates less essential, thereby reducing financial and preparation overheads and discomfort factors in gait studies.

Keywords: electromyography; inertial measurement units; gait-phase prediction; machine learning; Parkinson's disease

Citation: Haufe, S.; Isaias, I.U.; Pellegrini, F.; Palmisano, C. Gait Event Prediction Using Surface Electromyography in Parkinsonian Patients. *Bioengineering* **2023**, *10*, 212. https://doi.org/10.3390/bioengineering10020212

Academic Editor: Christina Zong-Hao Ma

Received: 3 January 2023
Revised: 31 January 2023
Accepted: 3 February 2023
Published: 6 February 2023

1. Introduction

Gait and balance disturbances are common and important clinical manifestations of Parkinson's disease (PD), leading to mobility impairment and falls [1]. Current treatments (pharmacological and deep brain stimulation (DBS)) provide only partial benefits in gait derangements in PD, with a wide variability in outcomes [2–5].

Despite detailed testing, specific factors that are critical to predicting locomotor deterioration in PD remain elusive [6–9]. Beside subtle onset and clinical heterogeneity [10], technical limitations have hampered the timely and direct recording of supraspinal locomotor derangements in these patients. Only recently have advances in portable electroencephalography systems [11,12] and new DBS devices capable of on-demand recording using chronically implanted electrodes (e.g., Activa PC+S and Percept PC (Medtronic PLC)

or AlphaDBS (Newronika Srl)) [13–15] enabled the recording of ongoing brain activity during actual gait in PD to be performed [16–18].

The precise assessment of gait dynamics should account for its context dependency. New study setups employing fully immersive virtual reality (VR) or augmented reality allow gait assessment (with optoelectronic systems, force plates, etc.) to be conducted in environments that deliver patient-specific triggers of gait impairment (e.g., [19]). These setups could facilitate the identification of biomarkers for the fine-tuning of therapy delivery, e.g., adaptive DBS programming and so-called VR Exposure Therapy [20].

An open challenge is the continuous monitoring of gait parameters in laboratory as well as real-world environments. Technically, parameters such as the timings of heel strike and toe-off events, which define swing and stance phases and provide valuable information about cadence patterns, etc., can be assessed with optoelectronic systems and force plates. Both systems, however, are expensive, require qualified personnel, and do not offer monitoring in ecological settings. Video-based analyses of gait have also been proposed [21], although it is unclear whether these could reach the required precision to identify individual events within a gait cycle, especially for clinical applications and in ecological settings. Wearable motion sensors such as inertial measurement units (IMUs) are another viable option to capture gait events in natural environments with high temporal accuracy [22,23]. However, they do not contain further neurophysiological information that may be crucial to understanding and predicting gait derangements [24]. Surface electromyography (EMG) provides the missing link between neural signals and kinematics that makes the comprehensive characterization of pathological gait possible. EMG measurements have been used to predict lower-limb motion in advance [25,26] for real-time control of a prosthesis [27–29] or adaptive DBS devices [16–18,25,26,30,31]. EMG profiles of the gait cycle have also been shown to anticipate specific gait derangements in PD, such as freezing of gait [32], a sudden episodic inability to produce effective stepping despite the intention to walk. The combined use of IMU and EMG signals would make the description of the motor actions and intentions underlying gait kinematic features and alterations possible.

However, some practical limitations should be considered when applying additional sensors on severely ill patients, especially when performing recordings after suspension of medications. For example, in patients with PD, the overnight suspension of dopaminergic drugs is fundamental to evoke and study PD-related symptoms but greatly reduces the time window available for experimental recordings. Limiting the preparation period by limiting the number of sensors may help considerably in this regard. In addition, an excessive number of sensors may alter the natural behavior of subjects, undermining the advantages of working in ecological environments. Another crucial aspect is the cost of multiple sets of sensors. Considering that probes comprising both IMUs and EMG are generally more expensive than standalone solutions, the need for IMUs and EMG in the fine-grained evaluation of gait may be a limiting factor for many laboratories and applications in clinical routine. The use of multiple devices may also not be practical in clinical routine, as synchronization or different recording software may be needed.

Considering this, the development of novel technologies that can extract multiple types of signals from the same set of sensors is highly desirable. While the same kinematics can be produced by different muscular patterns, lower-limb kinematics can be inferred using analysis of EMG [33]. The idea of detecting gait events directly using EMG signals, circumventing additional IMUs or force plates, is gaining traction [34–38]. Ziegier and colleagues [38] reported high accuracy in classifying stance and swing phases during human gait based on EMG recordings. They first extracted a weighted signal difference that exploits the difference in EMG activity between corresponding muscles of the two legs and then trained a support vector machine to classify the gait phases. Using a deep learning approach, Morbidoni and colleagues [35] were also able to classify stance and swing phases and predict foot–floor contacts under natural walking conditions in healthy subjects. Other studies showed similar results in learned and unlearned subjects [37], and using intra-subject training only [34]. This would not only simplify future recording setups

but also permit the re-analysis of EMG datasets recorded without IMUs or in cases of data loss due to technical problems with the IMU to be performed. This second scenario is particularly problematic when recordings cannot be repeated due to the patient's clinical condition. Additionally, the extraction and prediction of gait events using lower-limb EMG activity is of fundamental importance for the development of an EMG-driven prosthesis, where predicting the subsequent gait phase using muscular signals increases prosthesis efficiency and responsiveness [33].

Previous approaches aimed to predict discrete gait events (i.e., heel contact and toe-off), and little attention has been paid to reconstructing the time course of the relevant kinematic variables. Brantley and colleagues were able to predict knee and ankle kinematics, but with varying accuracy across trials and the subjects included [33]. In addition, most previous studies focused on treadmill walking, which may not capture the variability of ground walking [36–38]. Lastly, we are not aware of any approach that has been tested on unmedicated PD patients during long periods of continuous walking.

In the present study, we explore the possibility of identifying fundamental gait events from surface EMG in parkinsonian patients using a machine learning approach. Compared with previous studies, we did not frame the problem as one of detection (i.e., to identify the timings of a fixed set of events) or classification (i.e., to segment the data into contiguous gait phases). Instead, we used an innovative regression approach to approximate continuous angular velocity profiles as measured by IMUs. We consider this approach strictly more powerful and flexible than previous approaches, as access to the predicted IMU time series allows us not only to extract predetermined types of gait events but also biomechanical quantities such as joint angular velocity and further parameters on which our model has not been trained. Our study is further set apart from published work in that we focused on a clinical cohort rather than healthy participants. To our knowledge, our study is the first to demonstrate the feasibility of accurate gait parameter estimation using EMG in such a population. Remarkably, our approach accounts for the substantial across-patient variability observed in gait patterns of clinical populations, allowing it to be applied without any patient-specific calibration.

2. Materials and Methods

2.1. Participants

We recruited six patients with idiopathic PD according to the UK Brain Bank criteria who did not suffer from any other disease, including cognitive decline (i.e., Mini-Mental State Examination score of >27), vestibular disorders, and orthopedic impairments, that could interfere with walking. An additional inclusion criterion for this preliminary study was the ability of the patient to walk continuously and without assistance for at least three minutes. Disease severity was evaluated using MDS-Unified Parkinson's Disease Rating Scale motor part (UPDRS-III), and the stage of the disease was evaluated using the Hoehn and Yahr (H&Y) scale. Using items 3.15–3.17 of UPDRS-III (hands and feet), a sum rest tremor sub-score was created for the right and left sides separately. Similarly, a sum bradykinesia-rigidity score (items 3.3–3.8) was obtained for each side.

Demographic and clinical features are listed in Table 1. The study was approved by the Ethics Committee of University of Würzburg and conformed to the declaration of Helsinki. All patients gave their written informed consent to participate.

2.2. Experimental Setup and Procedure

Patients were investigated in a practical medication-off state, i.e., on the morning after overnight withdrawal (>12 h) of all dopaminergic drugs (meds-off). Kinematic data were recorded using two IMUs (Opal, APDM), at a sampling rate of 128 Hz, placed bilaterally on the outer anklebones. Each sensor was placed with its vertical axis aligned with the tibial anatomic axis. Surface leg muscle activity as measured by 10 EMG probes (FREEEMG 1000, BTS) was recorded bilaterally on tibialis anterior (Ta), soleus (S), gastrocnemius medialis (Gm), gastrocnemius lateralis (Gl), and vastus lateralis (Vl) at a sampling rate of 1000 Hz.

Two transistor–transistor logic signals (TTL) were provided at the beginning and end of each trial to both EMG and IMU devices to make data synchronization possible. Patients started walking barefoot after a verbal signal at their self-selected speed along a large ellipsoidal path of about 60 m in length (Figure 1). We recorded between three and six trials (243 $\pm$ 71 s in duration) of unperturbed, steady-state, overground walking according to the clinical condition of each subject. Overall, 26 walking trials with a total duration of 105 min were obtained.

Table 1. Demographic and clinical features. Meds-off: practical medication-off state, i.e., overnight withdrawal (>12 h) of all dopaminergic drugs. Meds-on: medication-on state 30–60 min after receiving 1 to 1.5 times the levodopa-equivalent of the morning dose. UPDRS-III is presented as total score/tremor sub-score left/tremor sub-score right/bradykinesia-rigidity sub-score left/bradykinesia-rigidity sub-score right. Abbreviations: Hoehn and Yahr stage (H&Y); Levodopa equivalent daily dose (LEDD); Unified Parkinson's Disease Rating Scale motor part (UPDRS-III).

	Gender	Age, Years	Age at Onset, Years	LEDD, mg	UPDRS-III Meds-off	UPDRS-III Meds-on	H&Y
WP1	M	46	36	1167	50/2/4/14/11	15/1/0/3/4	3
WP2	M	57	50	900	28/3/7/4/9	5/0/0/0/4	2
WP3	F	59	52	362	18/2/0/2/8	11/1/0/1/7	1
WP4	F	55	49	640	9/0/0/6/2	5/0/0/4/1	1
WP5	M	61	51	610	12/0/0/2/8	5/0/0/0/4	2
WP6	M	65	58	610	30/0/1/5/13	21/0/0/2/8	2

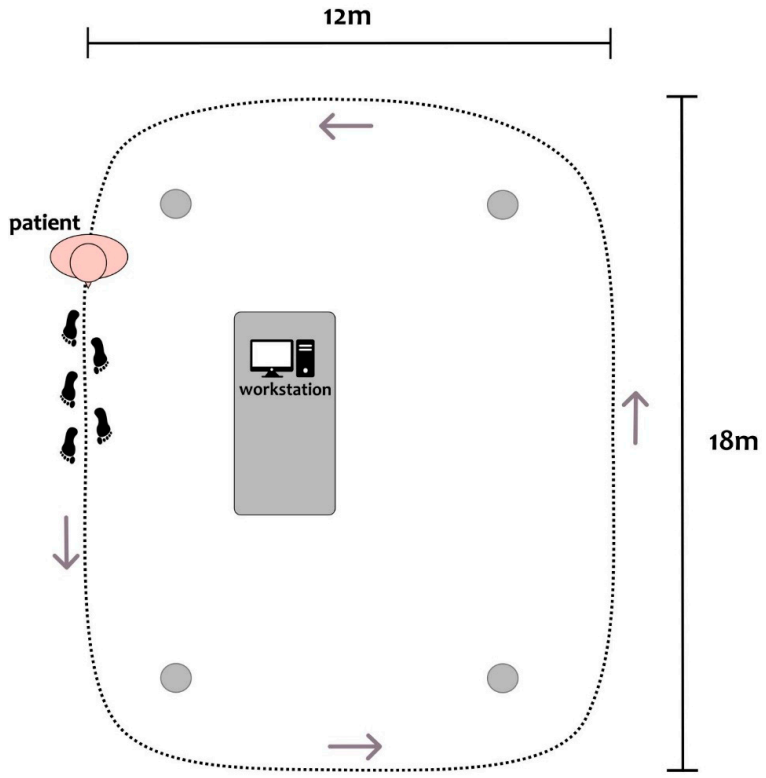

Figure 1. Top-view scheme of the experimental setup, with a patient depicted at the starting position of the circuit. Patients were asked to continuously walk along an elliptical circuit of approximately 60 m around the workstation. The inner boundary of the circuit was marked with four objects at its corners (gray dots). A clinician was close to the patient during all recordings.

2.3. Selection of EMG Channels

We focused on the muscles of the lower leg, which are highly involved during the gait cycle. Ta and S are distal monoarticular muscles with distinct and synergistic contributions to human gait [39]. According to [40], they are the most active muscles during gait and display the lowest inter-subject variability. We, therefore, hypothesized that models based on bilateral pairs of these muscles may be particularly suitable and potentially sufficient for predicting gait-related angular velocity profiles. The gastrocnemius muscle (biarticular) was added for a comprehensive evaluation of the triceps surae. Note that since medial and lateral gastrocnemii fulfill somewhat independent roles [41,42], both were added. Given the knee flexor activity of the gastrocnemius muscle, we then positioned the last available probe on the Vl, a major (monoarticular) knee extensor muscle.

Models based on different muscle combinations were compared to the model including all five pairs of muscles. We were interested in identifying minimal subsets of EMG probes that would make accurate IMU reconstruction possible. Thus, we further exhaustively tested all possible $2^5 - 1 = 31$ sets containing between one and five pairs of distinct muscles. Note that all considered models included either none or both the left and right EMG signals for each studied muscle. Thus, all models comprised an even number of muscles between two and ten.

2.4. Data Preprocessing

Figure 2 depicts a summary of data preprocessing (green box). EMG data were bandpass-filtered, rectified, and down-sampled to 200 Hz. IMU traces were up-sampled to 200 Hz using nearest-neighbor interpolation. IMU and EMG data were aligned to the rising edge of the first TTL signal for synchronization. A number of preprocessing steps were devised to facilitate the prediction of angular velocity traces from EMG data. To smooth out local extrema occurring due to noise, IMU data were processed with a moving-median filter with a 100 ms window length, followed by a moving-mean filter with a 40 ms window length. To achieve a similar degree of smoothness, EMG data were processed with a moving-median filter with a 200 ms window length, followed by a moving-mean filter with a 40 ms window length. All moving filters were centered. As a simple high-pass filter, the minimum in a moving window of 10 s in length was subtracted from the EMG data. To standardize scales across patients, EMG activation time courses were further normalized by subtracting the 1st percentile and dividing by the 95th percentile. Percentiles were estimated separately for each recording. Each recording was cropped to the exact on- and offsets of the walking period.

2.5. Extraction of Biomechanical Parameters

Swing peak velocity (SWP), heel contact (HC), and toe-off (TO) events were extracted from the angular velocity profiles measured with respect to the medio-lateral axis by the IMUs (see [43,44] for an extensive description of gait event detection using IMU data). This was performed separately for the left and right IMU sensors as follows: First, SWP events were identified as local maxima with at least 150°/s peak height and 0.7 s inter-peak distance. Two consecutive SWP events defined one gait cycle. Next, local minima within each cycle were used to define the corresponding HC and TO events. The HC event was defined as the earliest local minimum occurring in the sub-interval between 10% and 45% of the cycle. If no local minimum could be found, the global minimum within that sub-interval was used. Similarly, the TO events were defined as the latest local minimum occurring in the sub-interval between 55% and 90% of the cycle. Again, if no local minimum could be found, the global minimum within that sub-interval was used. At random, events extracted by the described algorithm were checked by an expert (C.P.) and were in agreement with manual determination based on the same IMU data. The procedure was used to define "ground-truth" gait events from recorded IMU data, as well as approximate event timings derived from reconstructed angular velocity time series based on EMG activity (see below; Figure 2, yellow and blue boxes).

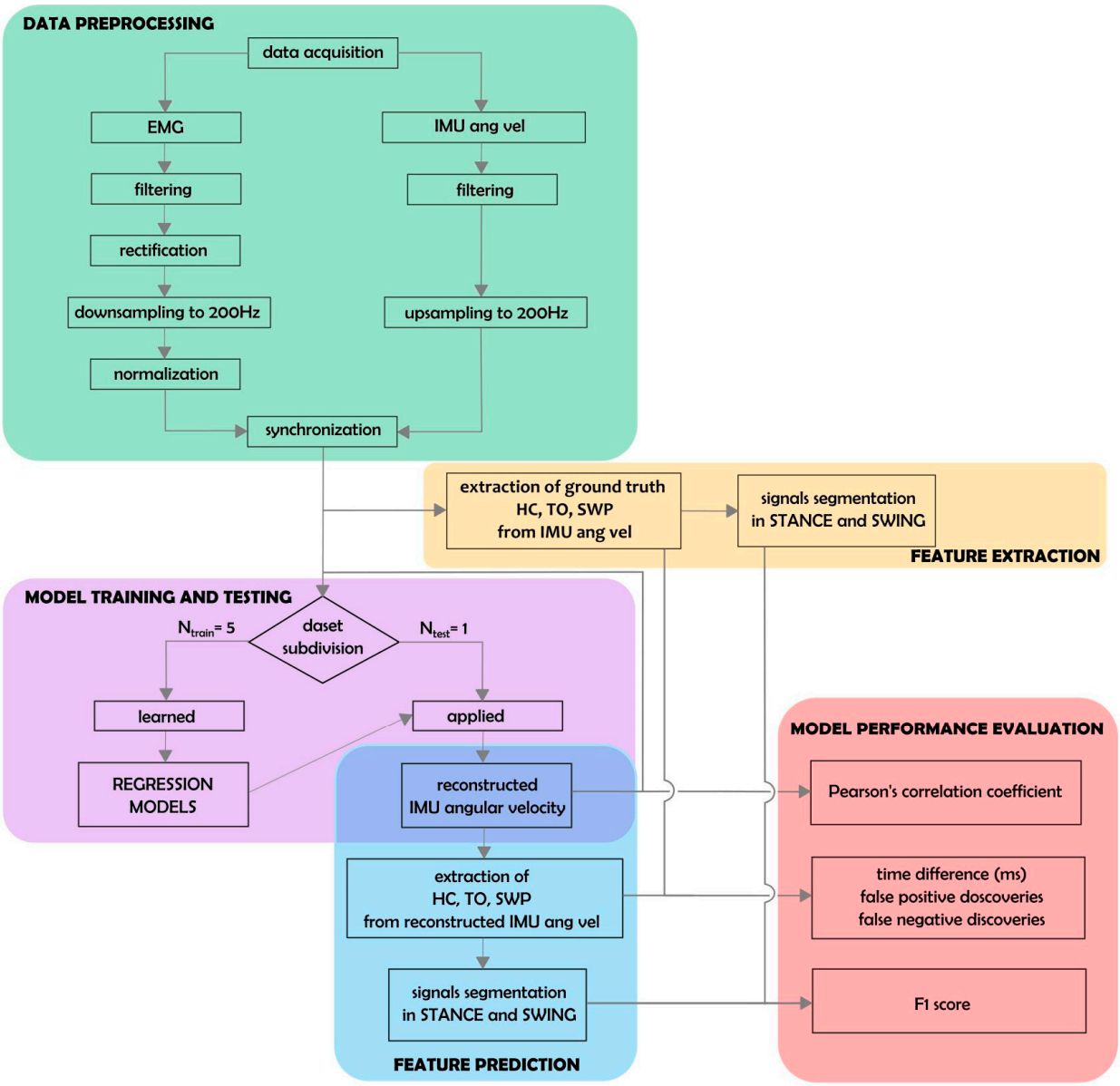

Figure 2. Schematic representation of data analysis. Thirty-one regression models corresponding to all possible muscle combinations were built and evaluated. Each model was trained on all patient data except for one, left out for the testing phase (N_{train} = 5, N_{test} = 1; pink box).

2.6. Prediction of Angular Velocity Profiles Using EMG

We used multiple linear regression to approximate the angular velocity with respect to the medio-lateral axis of the left and right ankle using the combined activation traces of multiple muscles within a window around the prediction point. The regression coefficients were fitted to minimize the mean-squared error between measured and approximated IMU traces on *training* data, consisting of pairs of IMU and EMG activity traces. To enable the prediction model to utilize the temporal dynamics of the EMG channels around the prediction time point, the temporal embedding of the EMG time series was performed. To this end, each selected EMG channel was complemented by temporally shifted versions $\tilde{x}_m(t) = [x_m(t+\tau_1), \ldots, x_m(t+\tau_K)]^T$, $m = 1, \ldots, M$, where $x_m(t+\tau)$ is the activity of the m-th EMG sensor at time $t+\tau$. Here, we used $K = 21$ equally spaced shifts, ranging from $\tau_1 = -500$ ms to $\tau_{21} = +500$ ms in steps of 50 ms. Thus, the prediction of the IMU signals at time t was based on EMG information within a window around t of one second in length. The relation between the embedded signal of all M EMG sensors,

$\widetilde{\boldsymbol{x}}(t) = [\widetilde{x}_1(t), \ldots, \widetilde{x}_M(t), 1]^T$ (including an offset term), and angular velocity $y(t)$ (either at the left or right ankle) was assumed to be linear according to the model $y(t) = \boldsymbol{\beta}^T\widetilde{\boldsymbol{x}}(t)$. The $(K{\cdot}M + 1)$-dimensional coefficient vector $\boldsymbol{\beta}^{OLS} = \left(\widetilde{\boldsymbol{X}}\widetilde{\boldsymbol{X}}^T\right)^{-1}\widetilde{\boldsymbol{X}}\boldsymbol{y}^T$ was estimated using ordinary least-squares (OLS) regression, where $\widetilde{\boldsymbol{X}} = [\widetilde{\boldsymbol{x}}(1), \ldots, \widetilde{\boldsymbol{x}}(T)]$, $\boldsymbol{y} = [y(1), \ldots, y(T)]$, and T denotes the number of available paired measurements of EMG and IMU activity in the training set. Using the fitted model, EMG-based IMU predictions were obtained as $\hat{y}(t) = \boldsymbol{\beta}^{OLS^T}\widetilde{\boldsymbol{x}}(t)$.

2.7. Performance Analysis

Models were evaluated exclusively on hold-out data using leave-one-patient-out cross-validation (Figure 2, pink and red boxes). Models were fitted on the concatenated trials of all but one patient (training data) and were evaluated on all trials of the held-out (test) patient, where each patient served as the hold-out patient once. This evaluation scheme provided unbiased assessment of prediction performance. Model predictions $\hat{y}(t) = \beta^T\widetilde{\boldsymbol{x}}^*(t)$ were obtained by multiplying coefficient vector β estimated using the training data to embedded EMG data $\widetilde{\boldsymbol{x}}^*(t)$ from each trial of the test patient.

Predicted and ground-truth data were compared on a per-trial and leg basis using the Pearson correlation coefficient (r). Gait events (SWP, HC, and TO) were extracted from the predicted IMU time series as described in Section 2.5. Separately for each leg, ground-truth and predicted HC and TO events were used to divide each trial into alternating segments representing the swing and stance phases of the gait cycle. The resulting binary time series were compared using the F1-score (see also [34]). In addition, the absolute displacement between matching true and predicted events was measured. Matching events were defined as those being <600 ms apart from each other. Predicted events lacking a matching ground-truth counterpart were counted as false detections. The false discovery rate (FDR) was defined per event type as the number of false detections divided by the number of total event detections. Conversely, true events lacking matching prediction were counted as false negatives (misses). The false-negative rate (FNR) for each event type was defined as the number of missed events divided by the total number of true events.

3. Results

Ninety-three minutes of gait activity and 5253 full gait cycles were analyzed across the six patients. The median gait cycle duration ranged from 1045 to 1140 ms, corresponding to cadences between 51 and 59 cycles per minute (see Table 2). The gait cycle duration variability was measured as the median absolute deviation from the median duration and ranged from 10 to 30 ms.

Figure 3 illustrates the average activation patterns of individual muscles (measured by means of EMG) relative to the angular velocity profiles (measured by the IMUs). The upper panels show the average IMU and EMG activity across the gait cycles of all patients as a function of time within a cycle. All ten muscles exhibited stable activation patterns relative to the individual gait events of both legs. Importantly, due to the stable timing of the gait cycle in patients with mild PD, the left leg muscles showed precise activation in well-defined time windows regarding HC and TO events of the left and right leg, and vice versa. The Vl displayed particularly consistent timings (as indicated by dark red colors) both for the left and right legs. The lower panels depict cross-correlations (computed on the concatenated data of all trials) of temporally shifted EMG activity traces relative to the IMU signal. The same 21 lags were analyzed, ranging from −500 ms to +500 ms relative to the IMU signal reported above for the machine learning models. Thus, the depicted correlograms represent the independent linear predictive quality of each of the 10 × 21 = 210 EMG features considered in our models, thereby indicating the influence of each muscle and delay combination for prediction (see also [45]). The activity profiles of all ten individual muscles showed substantial positive and negative correlations with the IMU signal within a window of 1 sec. The highest absolute correlations were observed for the Vl. Specifically, left Vl activity lagged behind the left IMU trace by 150 ms (r = 0.78) and

anticipated the right IMU trace by 350 ms (r = 0.76); in contrast, right Vl activity lagged behind the right IMU trace by 150 ms (r = 0.66) and anticipated the left IMU trace by 350 ms (r = 0.67). All reported cross-correlations were statistically significant ($p < 0.05$ after Bonferroni correction).

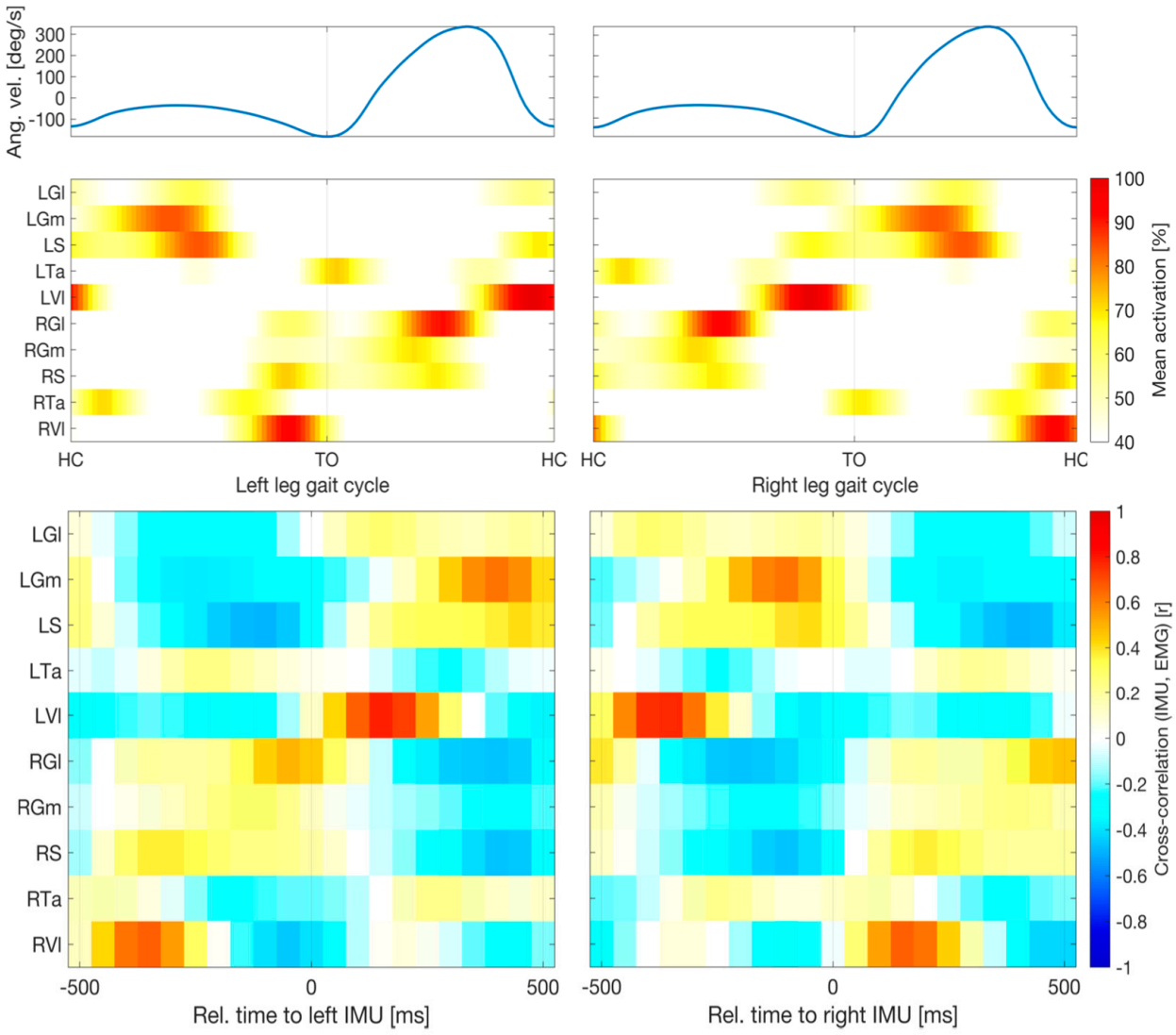

Figure 3. Relative timings of muscular and kinematic signals. Upper panels show average angular velocity measured by inertial measurement units (IMUs) and electromyographic (EMG) activity across all gait cycles of all patients as a function of time within a cycle. Percentages are relative to the 95th percentile of the raw data. Averages were cropped below 40%. All ten muscles exhibited stable activation patterns relative to the individual gait events of both legs. Lower panels depict cross-correlations (computed on the concatenated data of all trials) of temporally shifted EMG activity relative to the IMU signal. All ten muscles showed substantial absolute correlations with the IMU signal within a window of 1 sec. The highest correlations (Pearson correlation, r > 0.66) were observed for Vl activity with delays of 150 ms relative to the same leg or −350 ms relative to the opposing leg. Abbreviations: left and right gastrocnemius medialis (LGm and RGm) and lateralis (LGl and RGl); left and right soleus (LS and RS); left and right tibialis anterior (LTa and RTa); left and right vastus lateralis (LVl and RVl); TO, toe-off.

Table 2. Gait cycle statistics of individual patients.

	Median Gait Cycle Duration, ms	Cadence, Cycles/min	Gait Cycle Duration Variability, ms
WP1	1140	51	30
WP2	1050	57	15
WP3	1045	57	25
WP4	1080	54	30
WP5	1010	59	10
WP6	1095	55	25

Figure 4 shows an example segment of the preprocessed EMG and IMU data of one patient, the EMG-based predictions of the IMU time courses based on all ten available EMG probes, and the gait parameters extracted from true and predicted IMU time series. The EMG time courses of three selected individual muscles (bilateral Ta, S, and Vl) showed the clear periodic pattern of the gait cycle (bottom row). Out-of-sample predictions based on temporal embeddings of the activity of ten muscles showed a high correlation with the true IMU data (top row). Furthermore, gait events extracted from the predicted time series closely matched those extracted from the original IMU traces (top row). True and predicted gait phases based on the extracted events were consequently also closely aligned (center row). Results of similar quality were obtained when predictions were based on the left and right Vl only (see quantitative evaluation below).

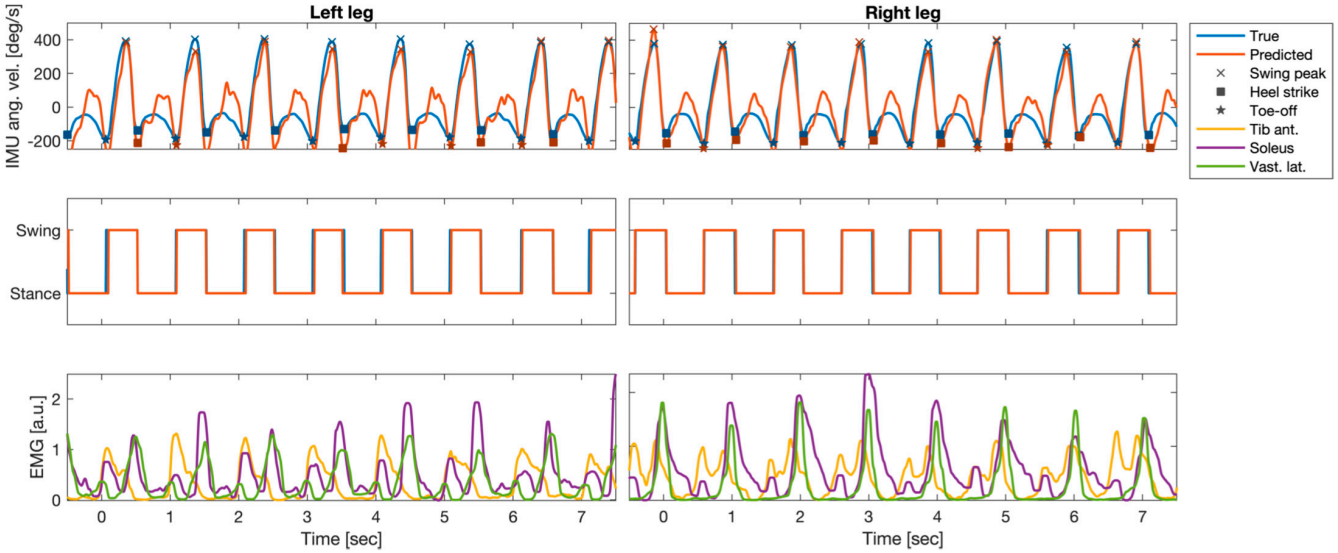

Figure 4. Example segment of preprocessed electromyography (EMG) and inertial measurement units (IMUs); angular velocity at the left and right anklebones (recordings of one patient (P5)), as well as the EMG-based predictions of the IMU time courses and the gait parameters extracted from true and predicted IMU time series. Top row: true IMU data and predictions derived from temporally embedded EMG activity of ten muscles. Predictions were derived from an ordinary least-squares regression model of fitted data of that had been fitted to data of the other five patients. Gait-related events (swing peak velocity (SWP), heel contact (HC), and toe-off (TO)) extracted from the predicted time series closely matched those extracted from the original IMU traces. Center row: True and predicted gait phases based on the extracted events were closely aligned. Bottom row: EMG time courses of three selected individual muscles (bilateral soleus, tibialis anterior, and vastus lateralis).

Figure 5 quantitatively summarizes the performance of EMG-based reconstructions of IMU time courses and gait events. The median (IQR across all 26 trials) Pearson correlation

between measured and reconstructed IMU time courses, based on all ten muscles, was r = 0.80 (0.74 to 0.87) for the left ankle and r = 0.85 (0.78 to 0.90) for the right ankle. Using the left and right Vl, the performance was on par, with r = 0.86 (0.78 to 0.88) for the left IMU probe and r = 0.83 (0.80 to 0.88) for the right IMU probe. Using the left and right Ta and S muscles did not lead to competitive performance, with r = 0.47 (0.35 to 0.66) for the left IMU and r = 0.55 (0.46 to 0.66) for the right IMU. Importantly, the combination of left and right Vl was found to be on par with the full model for all the performance metrics, whereas the combination of S and Ta was competitive in none. For this reason, we restricted our reporting to the model comprising left and right Vl. With few exceptions, gait events could be reconstructed with median absolute temporal displacements of <50 ms using IMU predictions derived from this model. The median (IQR) displacement for SWP was 40 (20 to 60) ms for the left leg and 38 (25 to 60) ms for right leg. For HC events, median temporal displacements were 35 (25 to 55) ms for the left leg and 45 (30 to 60) ms for the right leg. For TO events, median displacements were 43 (30 to 100) ms for the left leg and 43 (20 to 95) ms for the right leg. Segmentations of the recordings into dichotomous gait phases based on detected HC and TO events were similar for measured and reconstructed IMU data. Median (IQR) F1-scores were 0.89 (0.87 to 0.93) for the left leg and 0.89 (0.86 to 0.93) for the right leg.

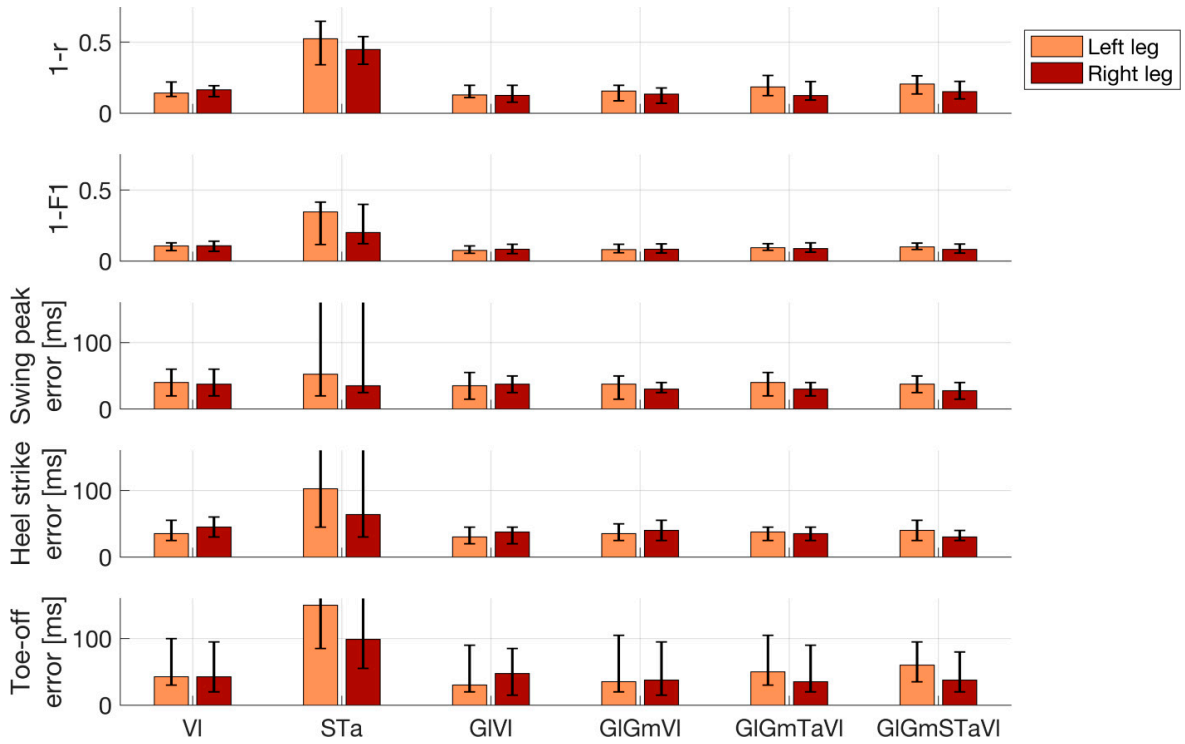

Figure 5. Performance of electromyography (EMG)-based reconstructions of inertial measurement unit (IMU) time courses and gait events. Lower numbers represent better performance. Top row: Pearson correlation (r) between measured and reconstructed angular velocity profiles of the left and right ankles. Second row: Accuracy of the reconstructed dichotomous (swing vs. stance) gait phases compared with the IMU-based ground truth, as measured by the F1-score. Bottom three rows: Absolute displacement of three types of events (swing peak velocity, heel contact, and toe-off) determined using reconstructed rather than measured IMU data. Results are shown separately for the left and right leg and for the best-performing prediction models utilizing between one and five pairs of EMG channels. In addition, results of the combination of the left and right soleus and tibialis anterior are also shown. Bar plots depict median performance across 26 walking trials of six patients in total, while overlaid whiskers depict first and third quartiles. Abbreviations: gastrocnemius medialis (Gm); lateralis (Gl); soleus (S); tibialis anterior (Ta); vastus lateralis (Vl).

Event detection errors were rare and did not occur in most trials. Across all trials, events were missed in 1.4% (n = 71; left leg) and 1.3% (n = 68; right leg) of cases. Numbers were nearly identical for all three event types, as HC and TO events were always determined relative to the two enclosing SWP events (see Section 2.5). False event discoveries were rare (<0.1% of the total events detected for both legs and all three event types). In absolute terms, between 2 and 4 out of over 5000 detected events were false discoveries.

4. Discussion

We have demonstrated the feasibility of accurately determining gait events such as HC and TO, defining the swing and stance phases of the gait cycle, in PD patients using a single pair of EMG probes placed bilaterally on the Vl muscle. Our proposed method may have substantial practical benefits in experimental setups in which EMG derivations are indispensable and where additional equipment for kinematic analysis (e.g., foot switches, IMUs, or a motion-capturing system) is either unavailable or would introduce undesired complexity, especially in severely ill patients. Furthermore, robust acquisition of EMG signals is necessary in experimental and commercial applications to achieve control of myoelectric interfaces for neuroprosthetics [29], including future adaptive DBS devices [30].

Rather than framing the prediction problem as one of binary classification [34], our approach consisted of two steps: First, the angular velocity at the left and right anklebones was predicted using the activity of between two and ten EMG probes. This mapping was learned a priori from training data for which both EMG and IMU recordings were available. Using carefully designed data features (temporally embedded, smoothed muscle activation time courses), a simple linear regression approach was found to be suitable to achieve sufficient reconstruction performance. Second, predefined rules were used to extract prominent events and the main phases of the gait cycle. These rules accommodate domain knowledge about the timing of events relative to each other, which constitutes a substantial advantage over algorithms that are completely naïve to the underlying data, framing gait cycle prediction as an abstract classification problem. Importantly, our approach does not require any calibration involving real IMU data, as models fitted a priori on a training cohort (e.g., the data reported here) can be readily applied to new patients. Due to the simplicity of our model, its application amounts to a simple linear filtering of the appropriately recorded and preprocessed EMG data and does not require any advanced machine learning software. In addition, our approach of approximating IMU time courses instead of individual events or categorial segmentation labels offers numerous additional advantages. These include the direct interpretation of the predicted time courses in terms of gait mechanics. Potential failure modes of the model (e.g., due to misplaced or noisy EMG probes) can easily be detected through visual inspection of the predicted time courses. Since SWP could be accurately detected even using reconstructed angular velocities and HC and TO were defined relative to SWP, our system achieved low numbers of event-detection errors and high overall accuracy regarding the determination of gait phases. It is also likely that our approach could be generalized to the extraction of other biomechanically relevant parameters of the upper and lower extremities.

Contrary to our prediction, the EMG profiles of the S and Ta muscles were insufficient to reliably identify major gait cycle events in parkinsonian patients. We based this hypothesis on the distinctive and synergistic activity of these two monoarticular (i.e., ankle) muscles during human locomotion. Indeed, normal EMG activity of the plantar flexors has been reported to mainly occur during the stance phase. In this phase, the triceps surae restrains the tibial rotation controlling for disequilibrium torque, which is responsible for propelling the body [46,47]. The ankle dorsi-flexors are instead mainly active during the swing phase, controlling for sufficient foot clearance, with an additional contribution in the loading response phase for the lowering of the foot to the ground after HC [48], thus assisting the forward momentum of the tibia during the heel rocker action at the ankle [49]. These muscles, however, may show large stride-to-stride variability in EMG profiles [48], especially in patients with PD [50,51]. In particular, a great intra- and inter-subject variabil-

ity of Ta activity during gait has been described in parkinsonian patients in the meds-off state [50].

The prediction model did not improve when replacing the S muscle with the Gm or Gl or by adding this muscle to the S-Ta pair (data not shown). This was unexpected because while the S muscle may provide less forward propulsion with physiological aging, the gastrocnemius muscle has been shown to maintain its contribution to initiating swinging limb movement [52,53], thus possibly allowing kinematic events to be more accurately detected. Rodriguez and colleagues demonstrated a simplification of modular control of locomotion in PD with individual muscle contribution of the gastrocnemius, but not the S, among ankle plantar flexors and the semimembranosus and biceps femoris for knee flexor musculature [54].

In our study, EMG recordings of the Vl provided the most accurate prediction of IMU times series and gait events. The action pattern of this muscle during the gait cycle paralleled the activation of the Ta but was more selectively confined to the HC. This muscle controls the knee flexion that occurs after HC and ensures knee extension during terminal swing to prepare for ground contact [49,55].

In principle, there are an infinite number of different combinations of muscle activation that can be applied to maintain a particular posture or produce a given movement [56]. However, despite the apparent redundancy, four or five component activity patterns may be distributed to all the muscles that are specifically activated during locomotion; thus, the activation of each muscle involves a dynamic weighting of these basic patterns [57,58]. Interestingly, Ta, S, and Vl contributed differently to these factors [57,58]. Our results suggest that characteristic activity patterns of one pair—left and right Vl—are sufficient for the proper detection of gait events in patients with PD (H&Y: I–III).

Limitations

Our study is somewhat limited by the fact that IMU data are not considered the "gold standard" for defining ground-truth gait parameters. Force plates would have allowed the precise detection of HC and TO events, and possibly of the individual muscle contribution to ground reaction forces, to be performed [59,60]. However, it would have been impracticable to record the high number of steps and total gait time acquired in our study using force plates. IMU systems are sufficiently accurate in the assessment of fundamental gait spatiotemporal parameters [23,61] and have previously been used as ground truth for gait event detection [62]. Furthermore, they allow the SWP event to be detected, which cannot be captured by ground devices, foot switches, or insole pressure sensors.

The proposed approach was not tested on healthy control data. However, we expect our model to effectively predict gait events in healthy controls, as patient data are more heterogeneous and generally more challenging in terms of gait alterations, and inter-subject and inter-trial variability, as well as artifact contamination.

We were also only able to recruit a few patients for this study. However, it should be considered that walking for over three minutes in the meds-off state is very challenging for subjects with PD and greatly limited patient recruitment. Another limitation was the relatively homogeneous walking speed across all patients. We preferred not to alter the patients' natural speed, because we wanted to test our model in an ecological setup. In addition, the meds-off state limited the recording window and the possibility of exploring more than one gait condition. It is thus presently unclear how well our prediction model would perform for different speeds when applied out of the box. However, it is straightforward to adapt the model to different speeds by either temporally adjusting the embedding delays ($\tau_1, \ldots, \tau_K$) of test participants to their individual walking speed or retraining the model on data with matching speed.

5. Conclusions

We have demonstrated the accurate and robust detection of gait events in six parkinsonian patients using just two EMG probes placed on the left and right vastus lateralis. Unlike solutions presented in previous work, our approach proceeds in two steps: First, IMU time courses are predicted using EMG activity within a surrounding temporal window using multiple linear regressions. Second, gait parameters such as heel strike and toe-off events are extracted from the predicted time series. This approach led to accurate results and has the advantage over previous ones that discrete gait events and continuous time series of relevant kinematic quantities can be predicted. It is further expected that it could be generalized to the extraction of further gait parameters not considered here without any model retraining. Our model and an example dataset, as well as Matlab code for data preprocessing, model training, model evaluation, and plotting, have been made publicly available under https://github.com/braindatalab/EMGgaitprediction (accessed on 4 February 2023). Our approach may have practical benefits for gait studies in which the application of multiple sensing devices is considered impractical, troublesome, or too expensive. Notably, our model was validated using a leave-one-patient-out strategy. We observed very good performance in held-out patients, demonstrating that the model is able to accommodate the across-patient variability of the studied clinical population. Future work could adapt our approach to varying walking speeds and may further extend it to the prediction of other kinematic data obtained using EMG.

Author Contributions: Conceptualization, S.H. and I.U.I.; methodology, S.H., C.P. and I.U.I.; software, S.H.; formal analysis, S.H. and F.P.; investigation, C.P. and I.U.I.; resources, S.H., C.P. and I.U.I.; data curation, C.P.; writing—original draft preparation, S.H. and I.U.I.; writing—review and editing, S.H., C.P., F.P. and I.U.I.; visualization, S.H. and C.P.; supervision, C.P.; project administration, I.U.I.; funding acquisition, S.H., C.P. and I.U.I. All authors have read and agreed to the published version of the manuscript.

Funding: This study was sponsored by Deutsche Forschungsgemeinschaft (DFG; German Research Foundation) Project-ID 424778381-TRR 295 and Fondazione Grigioni per il Morbo di Parkinson. S.H. received funding from the European Research Council (ERC) under the European Union's Horizon 2020 research and innovation program (grant agreement No. 758985). C.P. was supported by a grant from German Excellence Initiative to the Graduate School of Life Sciences, University of Würzburg. I.U.I. received funding from New York University School of Medicine and The Marlene and Paolo Fresco Institute for Parkinson's and Movement Disorders, which was made possible with support from Marlene and Paolo Fresco.

Institutional Review Board Statement: The study was conducted in accordance with the Declaration of Helsinki and approved by the Ethics Committee of University of Würzburg (Nos. 103/20 and 36/17).

Informed Consent Statement: Informed consent was obtained from all subjects involved in the study.

Data Availability Statement: The data presented in this study are available upon request from the corresponding author. The data are not publicly available for privacy reasons.

Acknowledgments: We would like to thank all patients and caregivers for their participation. The draft manuscript was edited for English language by Deborah Nock (Medical WriteAway, Norwich, UK).

Conflicts of Interest: The authors declare no conflict of interest. The funders had no role in the design of the study; in the collection, analyses, or interpretation of data; in the writing of the manuscript; or in the decision to publish the results.

References

1. Wood, B.H.; Bilclough, J.A.; Bowron, A.; Walker, R.W. Incidence and Prediction of Falls in Parkinson's Disease: A Prospective Multidisciplinary Study. *J. Neurol. Neurosurg. Psychiatry* **2002**, *72*, 721–725. [CrossRef] [PubMed]
2. Giladi, N.; Balash, J.; Hausdorff, J.M. *Gait Disturbances in Parkinson's Disease BT—Mapping the Progress of Alzheimer's and Parkinson's Disease*; Mizuno, Y., Fisher, A., Hanin, I., Eds.; Springer US: Boston, MA, USA, 2002; pp. 329–335. ISBN 978-0-306-47593-1.

3. Pötter-Nerger, M.; Volkmann, J. Deep Brain Stimulation for Gait and Postural Symptoms in Parkinson's Disease. *Mov. Disord.* **2013**, *28*, 1609–1615. [CrossRef]
4. Karachi, C.; Cormier-Dequaire, F.; Grabli, D.; Lau, B.; Belaid, H.; Navarro, S.; Vidailhet, M.; Bardinet, E.; Fernandez-Vidal, S.; Welter, M.-L. Clinical and Anatomical Predictors for Freezing of Gait and Falls after Subthalamic Deep Brain Stimulation in Parkinson's Disease Patients. *Park. Relat. Disord.* **2019**, *62*, 91–97. [CrossRef]
5. Curtze, C.; Nutt, J.G.; Carlson-Kuhta, P.; Mancini, M.; Horak, F.B. Levodopa Is a Double-Edged Sword for Balance and Gait in People With Parkinson's Disease. *Mov. Disord.* **2015**, *30*, 1361–1370. [CrossRef]
6. Creaby, M.W.; Cole, M.H. Gait Characteristics and Falls in Parkinson's Disease: A Systematic Review and Meta-Analysis. *Park. Relat. Disord.* **2018**, *57*, 1–8. [CrossRef]
7. Palmisano, C.; Brandt, G.; Pozzi, N.G.; Alice, L.; Maltese, V.; Andrea, C.; Jens, V.; Pezzoli, G.; Frigo, C.A.; Isaias, I.U. Sit-to-Walk Performance in Parkinson's Disease: A Comparison between Faller and Non-Faller Patients. *Clin. Biomech.* **2019**, *63*, 140–146. [CrossRef] [PubMed]
8. Dipaola, M.; Pavan, E.E.; Cattaneo, A.; Frazzitta, G.; Pezzoli, G.; Cavallari, P.; Frigo, C.A.; Isaias, I.U. Mechanical Energy Recovery during Walking in Patients with Parkinson Disease. *PLoS ONE* **2016**, *11*, e0156420. [CrossRef] [PubMed]
9. Isaias, I.U.; Volkmann, J.; Marzegan, A.; Marotta, G.; Cavallari, P.; Pezzoli, G. The Influence of Dopaminergic Striatal Innervation on Upper Limb Locomotor Synergies. *PLoS ONE* **2012**, *7*, e51464. [CrossRef]
10. Mirelman, A.; Bonato, P.; Camicioli, R.; Ellis, T.D.; Giladi, N.; Hamilton, J.L.; Hass, C.J.; Hausdorff, J.M.; Pelosin, E.; Almeida, Q.J. Gait Impairments in Parkinson's Disease. *Lancet Neurol.* **2019**, *18*, 697–708. [CrossRef]
11. Nordin, A.D.; Hairston, W.D.; Ferris, D.P. Dual-Electrode Motion Artifact Cancellation for Mobile Electroencephalography. *J. Neural Eng.* **2018**, *15*, 056024. [CrossRef]
12. Jacobsen, N.S.J.; Blum, S.; Witt, K.; Debener, S. A Walk in the Park? Characterizing Gait-Related Artifacts in Mobile EEG Recordings. *Eur. J. Neurosci.* **2020**, *54*, 8421–8440. [CrossRef] [PubMed]
13. Arlotti, M.; Palmisano, C.; Minafra, B.; Todisco, M.; Pacchetti, C.; Canessa, A.; Pozzi, N.G.; Cilia, R.; Prenassi, M.; Marceglia, S.; et al. Monitoring Subthalamic Oscillations for 24 Hours in a Freely Moving Parkinson's Disease Patient. *Mov. Disord.* **2019**, *34*, 757–759. [CrossRef] [PubMed]
14. Canessa, A.; Pozzi, N.G.; Arnulfo, G.; Brumberg, J.; Reich, M.M.; Pezzoli, G.; Ghilardi, M.F.; Matthies, C.; Steigerwald, F.; Volkmann, J.; et al. Striatal Dopaminergic Innervation Regulates Subthalamic Beta-Oscillations and Cortical-Subcortical Coupling during Movements: Preliminary Evidence in Subjects with Parkinson's Disease. *Front. Hum. Neurosci.* **2016**, *10*, 611. [CrossRef] [PubMed]
15. Thenaisie, Y.; Palmisano, C.; Canessa, A.; Keulen, B.J.; Capetian, P.; Jiménez, M.C.; Bally, J.F.; Manferlotti, E.; Beccaria, L.; Zutt, R.; et al. Towards Adaptive Deep Brain Stimulation: Clinical and Technical Notes on a Novel Commercial Device for Chronic Brain Sensing. *J. Neural Eng.* **2021**, medRxiv:2021.03.10.21251638. [CrossRef] [PubMed]
16. Pozzi, N.G.; Canessa, A.; Palmisano, C.; Brumberg, J.; Steigerwald, F.; Reich, M.M.; Minafra, B.; Pacchetti, C.; Pezzoli, G.; Volkmann, J.; et al. Freezing of Gait in Parkinson's Disease Reflects a Sudden Derangement of Locomotor Network Dynamics. *Brain* **2019**, *142*, 2037–2050. [CrossRef]
17. Arnulfo, G.; Pozzi, N.G.; Palmisano, C.; Leporini, A.; Canessa, A.; Brumberg, J.; Pezzoli, G.; Matthies, C.; Volkmann, J.; Isaias, I.U. Phase Matters: A Role for the Subthalamic Network during Gait. *PLoS ONE* **2018**, *13*, 1–19. [CrossRef]
18. Canessa, A.; Palmisano, C.; Isaias, I.U.; Mazzoni, A. Gait-Related Frequency Modulation of Beta Oscillatory Activity in the Subthalamic Nucleus of Parkinsonian Patients. *Brain Stimulation* **2020**, *13*, 1743–1752. [CrossRef]
19. Palmisano, C.; Kullmann, P.; Hanafi, I.; Verrecchia, M.; Latoschik, M.E.; Canessa, A.; Fischbach, M.; Isaias, I.U. A Fully-Immersive Virtual Reality Setup to Study Gait Modulation. *Front. Hum. Neurosci.* **2022**, *16*, 783452. [CrossRef]
20. Dockx, K.; Bekkers, E.M.; Van den Bergh, V.; Ginis, P.; Rochester, L.; Hausdorff, J.M.; Mirelman, A.; Nieuwboer, A. Virtual Reality for Rehabilitation in Parkinson's Disease. *Cochrane Database Syst. Rev.* **2016**, *12*, CD010760. [CrossRef]
21. Sampath Dakshina Murthy, A.; Karthikeyan, T.; Vinoth Kanna, R. Gait-Based Person Fall Prediction Using Deep Learning Approach. *Soft Comput.* **2022**, *26*, 12933–12941. [CrossRef]
22. Anwary, A.R.; Yu, H.; Vassallo, M. Optimal Foot Location for Placing Wearable IMU Sensors and Automatic Feature Extraction for Gait Analysis. *IEEE Sens. J.* **2018**, *18*, 2555–2567. [CrossRef]
23. Zago, M.; Sforza, C.; Pacifici, I.; Cimolin, V.; Camerota, F.; Celletti, C.; Condoluci, C.; De Pandis, M.F.; Galli, M. Gait Evaluation Using Inertial Measurement Units in Subjects with Parkinson's Disease. *J. Electromyogr. Kinesiol.* **2018**, *42*, 44–48. [CrossRef] [PubMed]
24. Yokoyama, H.; Yoshida, T.; Zabjek, K.; Chen, R.; Masani, K. Defective Corticomuscular Connectivity during Walking in Patients with Parkinson's Disease. *J. Neurophysiol.* **2020**, *124*, 1399–1414. [CrossRef] [PubMed]
25. Wentink, E.C.; Schut, V.G.H.; Prinsen, E.C.; Rietman, J.S.; Veltink, P.H. Detection of the Onset of Gait Initiation Using Kinematic Sensors and EMG in Transfemoral Amputees. *Gait Posture* **2014**, *39*, 391–396. [CrossRef]
26. Wentink, E.C.; Beijen, S.I.; Hermens, H.J.; Rietman, J.S.; Veltink, P.H. Intention Detection of Gait Initiation Using EMG and Kinematic Data. *Gait Posture* **2013**, *37*, 223–228. [CrossRef]
27. Zhang, F.; Huang, H. Source Selection for Real-Time User Intent Recognition toward Volitional Control of Artificial Legs. *IEEE J. Biomed. Health Inform.* **2013**, *17*, 907–914. [CrossRef]

28. Huang, H.; Zhang, F.; Hargrove, L.J.; Dou, Z.; Rogers, D.R.; Englehart, K.B. Continuous Locomotion-Mode Identification for Prosthetic Legs Based on Neuromuscular-Mechanical Fusion. *IEEE Trans. Bio-Med. Eng.* **2011**, *58*, 2867–2875. [CrossRef]
29. Ison, M.; Artemiadis, P. The Role of Muscle Synergies in Myoelectric Control: Trends and Challenges for Simultaneous Multifunction Control. *J. Neural Eng.* **2014**, *11*, 051001. [CrossRef]
30. Vissani, M.; Isaias, I.U.; Mazzoni, A. Deep Brain Stimulation: A Review of the Open Neural Engineering Challenges. *J. Neural Eng.* **2020**, *17*, 051002. [CrossRef]
31. Swann, N.C.; de Hemptinne, C.; Miocinovic, S.; Qasim, S.; Ostrem, J.L.; Galifianakis, N.B.; Luciano, M.S.; Wang, S.S.; Ziman, N.; Taylor, R.; et al. Chronic Multisite Brain Recordings from a Totally Implantable Bidirectional Neural Interface: Experience in 5 Patients with Parkinson's Disease. *J. Neurosurg.* **2018**, *128*, 605–616. [CrossRef]
32. Nieuwboer, A.; Dom, R.; De Weerdt, W.; Desloovere, K.; Janssens, L.; Stijn, V. Electromyographic Profiles of Gait Prior to Onset of Freezing Episodes in Patients with Parkinson's Disease. *Brain* **2004**, *127*, 1650–1660. [CrossRef]
33. Brantley, J.A.; Luu, T.P.; Nakagome, S.; Contreras-Vidal, J.L. Prediction of Lower-Limb Joint Kinematics from Surface EMG during Overground Locomotion. In Proceedings of the 2017 IEEE International Conference on Systems, Man, and Cybernetics (SMC), Banff, AB, Canada, 5–8 October 2017; pp. 1705–1709.
34. Di Nardo, F.; Morbidoni, C.; Mascia, G.; Verdini, F.; Fioretti, S. Intra-Subject Approach for Gait-Event Prediction by Neural Network Interpretation of EMG Signals. *BioMedical Eng. Online* **2020**, *19*, 58. [CrossRef]
35. Morbidoni, C.; Cucchiarelli, A.; Fioretti, S.; Di Nardo, F. A Deep Learning Approach to EMG-Based Classification of Gait Phases during Level Ground Walking. *Electronics* **2019**, *8*, 894. [CrossRef]
36. Meng, M.; She, Q.; Gao, Y.; Luo, Z. EMG Signals Based Gait Phases Recognition Using Hidden Markov Models. In Proceedings of the 2010 IEEE International Conference on Information and Automation, ICIA 2010, Harbin, China, 20–23 June 2010; pp. 852–856. [CrossRef]
37. Nazmi, N.; Abdul Rahman, M.A.; Yamamoto, S.I.; Ahmad, S.A. Walking Gait Event Detection Based on Electromyography Signals Using Artificial Neural Network. *Biomed. Signal Process. Control* **2019**, *47*, 334–343. [CrossRef]
38. Ziegier, J.; Gattringer, H.; Mueller, A. Classification of Gait Phases Based on Bilateral EMG Data Using Support Vector Machines. In Proceedings of the IEEE RAS and EMBS International Conference on Biomedical Robotics and Biomechatronics, Enschede, The Netherlands, 26–29 August 2018; pp. 978–983. [CrossRef]
39. Crenna, P.; Frigo, C. A Motor Programme for the Initiation of Forward-Oriented Movements in Humans. *J. Physiol.* **1991**, *437*, 635–653. [CrossRef]
40. Winter, D.A.; Yack, H.J. EMG Profiles during Normal Human Walking: Stride-to-Stride and Inter-Subject Variability. *Electroencephalogr. Clin. Neurophysiol.* **1987**, *67*, 402–411. [CrossRef]
41. Ahn, A.N.; Kang, J.K.; Quitt, M.A.; Davidson, B.C.; Nguyen, C.T. Variability of Neural Activation during Walking in Humans: Short Heels and Big Calves. *Biol. Lett.* **2011**, *7*, 7539–7542. [CrossRef]
42. Hug, F.; Del Vecchio, A.; Avrillon, S.; Farina, D.; Tucker, K. Muscles from the Same Muscle Group Do Not Necessarily Share Common Drive: Evidence from the Human Triceps Surae. *J. Appl. Physiol.* **2021**, *130*, 342–354. [CrossRef]
43. Rueterbories, J.; Spaich, E.G.; Larsen, B.; Andersen, O.K. Methods for Gait Event Detection and Analysis in Ambulatory Systems. *Med. Eng. Phys.* **2010**, *32*, 545–552. [CrossRef]
44. Cereatti, A.; Trojaniello, D.; Croce, U. Della Accurately Measuring Human Movement Using Magneto-Inertial Sensors: Techniques and Challenges. In Proceedings of the 2nd IEEE International Symposium on Inertial Sensors and Systems, IEEE ISISS 2015—Proceedings, Hapuna Beach, HI, USA, 23–26 March 2015; pp. 15–18. [CrossRef]
45. Haufe, S.; Meinecke, F.; Görgen, K.; Dähne, S.; Haynes, J.D.; Blankertz, B.; Bießmann, F. On the Interpretation of Weight Vectors of Linear Models in Multivariate Neuroimaging. *NeuroImage* **2014**, *87*, 96–110. [CrossRef]
46. Honeine, J.L.; Schieppati, M.; Gagey, O.; Do, M.C. The Functional Role of the Triceps Surae Muscle during Human Locomotion. *PLoS ONE* **2013**, *8*. [CrossRef]
47. Honeine, J.-L.; Schieppati, M.; Gagey, O.; Do, M.-C. By Counteracting Gravity, Triceps Surae Sets Both Kinematics and Kinetics of Gait. *Physiol. Rep.* **2014**, *2*, e00229. [CrossRef] [PubMed]
48. Di Nardo, F.; Ghetti, G.; Fioretti, S. Assessment of the Activation Modalities of Gastrocnemius Lateralis and Tibialis Anterior during Gait: A Statistical Analysis. *J. Electromyogr. Kinesiol.* **2013**, *23*, 1428–1433. [CrossRef] [PubMed]
49. Chleboun, G.S.; Busic, A.B.; Graham, K.K.; Stuckey, H.A. Fascicle Length Change of the Human Tibialis Anterior and Vastus Lateralis during Walking. *J. Orthop. Sport. Phys. Ther.* **2007**, *37*, 372–379. [CrossRef]
50. Caliandro, P.; Ferrarin, M.; Cioni, M.; Bentivoglio, A.R.; Minciotti, I.; D'Urso, P.I.; Tonali, P.A.; Padua, L. Levodopa Effect on Electromyographic Activation Patterns of Tibialis Anterior Muscle during Walking in Parkinson's Disease. *Gait Posture* **2011**, *33*, 436–441. [CrossRef] [PubMed]
51. Islam, A.; Alcock, L.; Nazarpour, K.; Rochester, L.; Pantall, A. Effect of Parkinson's Disease and Two Therapeutic Interventions on Muscle Activity during Walking: A Systematic Review. *Npj Park. Dis.* **2020**, *6*, 22. [CrossRef]
52. Neptune, R.R.; Kautz, S.A.; Zajac, F.E. Contributions of the Individual Ankle Plantar Flexors to Support, Forward Progression and Swing Initiation during Walking. *J. Biomech.* **2001**, *34*, 1387–1398. [CrossRef]
53. Schmitz, A.; Silder, A.; Heiderscheit, B.; Mahoney, J.; Thelen, D.G. Differences in Lower-Extremity Muscular Activation during Walking between Healthy Older and Young Adults. *J. Electromyogr. Kinesiol.* **2009**, *19*, 1085–1091. [CrossRef]

54. Rodriguez, K.L.; Roemmich, R.T.; Cam, B.; Fregly, B.J.; Hass, C.J. Persons with Parkinson's Disease Exhibit Decreased Neuromuscular Complexity during Gait. *Clin. Neurophysiol.* **2013**, *124*, 1390–1397. [CrossRef] [PubMed]
55. Cioni, M.; Richards, C.L.; Malouin, F.; Bedard, P.J.; Lemieux, R. Characteristics of the Electromyographic Patterns of Lower Limb Muscles during Gait in Patients with Parkinson's Disease When OFF and ON L-Dopa Treatment. *Ital. J. Neurol. Sci.* **1997**, *18*, 195–208. [CrossRef] [PubMed]
56. Guigon, E. Models and Architectures for Motor ControlSimple or Complex? In *Motor Control*; Danion, F., Mark, L., Eds.; Oxford University Press: Oxford, UK, 2010; pp. 478–502. ISBN 978-0-19-539527-3.
57. Ivanenko, Y.P.; Poppele, R.E.; Lacquaniti, F. Five Basic Muscle Activation Patterns Account for Muscle Activity during Human Locomotion. *J. Physiol.* **2004**, *556*, 267–282. [CrossRef]
58. Roemmich, R.T.; Fregly, B.J.; Hass, C.J. Neuromuscular Complexity during Gait Is Not Responsive to Medication in Persons with Parkinson's Disease. *Ann. Biomed. Eng.* **2014**, *42*, 1901–1912. [CrossRef] [PubMed]
59. Moissenet, F.; Dumas, R. Individual Contributions of the Lower Limb Muscles to the Position of the Centre of Pressure during Gait. *Comput. Methods Biomech. Biomed. Eng.* **2017**, *20*, 137–138. [CrossRef]
60. Farinelli, V.; Hosseinzadeh, L.; Palmisano, C.; Frigo, C. An Easily Applicable Method to Analyse the Ankle-Foot Power Absorption and Production during Walking. *Gait Posture* **2019**, *71*, 56–61. [CrossRef] [PubMed]
61. Storm, F.A.; Buckley, C.J.; Mazzà, C. Gait Event Detection in Laboratory and Real Life Settings: Accuracy of Ankle and Waist Sensor Based Methods. *Gait Posture* **2016**, *50*, 42–46. [CrossRef] [PubMed]
62. Storm, F.A.; Heller, B.W.; Mazzà, C. Step Detection and Activity Recognition Accuracy of Seven Physical Activity Monitors. *PLoS ONE* **2015**, *10*, e0118723. [CrossRef]